

Joint DOA and Non-circular Phase Estimation of Non-circular Signals for Antenna Arrays: Block Sparse Bayesian Learning Method

Zihan Shen, Jiaqi Li*, Xudong Dong and Xiaofei Zhang

Abstract—This letter proposes a block sparse Bayesian learning (BSBL) algorithm of non-circular (NC) signals for direction-of-arrival (DOA) estimation, which is suitable for arbitrary unknown NC phases. The block sparse NC signal representation model is constructed through a permutation strategy, capturing the available intra-block structure information to enhance recovery performance. After that, we create the sparse probability model and derive the cost function under BSBL framework. Finally, the fast marginal likelihood maximum (FMLM) algorithm is introduced, enabling the rapid implementation of signal recovery by the addition and removal of basis functions. Simulation results demonstrate the effectiveness and the superior performance of our proposed method.

Index Terms—Direction of arrival estimation, block sparse Bayesian learning, non-circular signals, fast marginal likelihood maximum.

I. INTRODUCTION

CONVENTIONAL subspace-based algorithms, such as multiple signal classification (MUSIC) [1], estimation of signal parameters via rotational invariance techniques (ES-PRIT) [2], and their variants like root-MUSIC [3] and TLS-ESPRIT [4], are widely used for direction-of-arrival (DOA) estimation due to their high resolution. However, their performance critically depends on the number of snapshots and array elements [5].

Emerging algorithms based on sparse signal representation (SSR) models, such as ℓ_p -norm ($0 < p \leq 1$) methods and greedy algorithms, frame DOA estimation as a sparse reconstruction problem for high accuracy [6], [7]. Compared with the aforementioned algorithms, sparse Bayesian learning (SBL) achieves the global minimum at the sparsest solution with fewer local minima [8]–[10]. Zhang et al. enhances the SBL with the block sparse Bayesian learning (BSBL) model, incorporating a block correlation matrix for improved accuracy [11]. The multiple measurement vector (MMV) model is transformed into a single measurement vector (SMV) model, culminating in the development of the T-SBL algorithm [12].

Utilizing waveform characteristics can enhance DOA estimation performance, particularly with non-circular (NC) sig-

This work was supported in part by National Natural Science Foundation of China under Grants 62371225, 62371227. (Corresponding author: Jiaqi Li)

Zihan Shen, Jiaqi Li, and Xiaofei Zhang are with the Key Laboratory of Dynamic Cognitive System of Electromagnetic Spectrum Space, Nanjing University of Aeronautics and Astronautics, Nanjing 211106, China (e-mail: shen-zihan@nuaa.edu.cn, lijiaqi2000@outlook.com, zhangxiaofei@nuaa.edu.cn).

Xudong Dong is with the College of Communication Engineering, Hangzhou Dianzi University, Hangzhou 310018, China (e-mail: dxd@hdu.edu.cn).

nals like multiple amplitude shift key (MASK) and binary phase shift key (BPSK), which exhibit unique properties including non-zero pseudo-covariance [13]–[15]. Several studies have proposed SBL algorithms for estimating NC signals [16], [17]. However, these algorithms often operate under the assumption of zero and identical NC phases, which is impractical in real-world scenarios. Yuan et al. [18] suggests that block sparsity can address this issue, but their method fails to accurately capture block sparsity or estimate NC phases.

This letter proposes an efficient DOA estimation algorithm of NC signals, enabling simultaneous recovery for DOA and NC phases within the BSBL framework. This algorithm constructs a block sparse model via a customized permutation matrix and then formulates a cost function using SBL and Type-II maximum likelihood [11]. Finally the desired parameters are estimated through fast marginal likelihood maximization (FMLM). Key contributions summarized as follows:

- 1) We correct the defective SSR based NC signals model proposed in [18] and construct an accurate one by our proposed permutation strategy.
- 2) To recover DOA and unknown NC phases simultaneously, the block sparse Bayesian inference is leveraged and validated through simulations.
- 3) To reduce computational complexity, the FMLM algorithm is introduced, accelerating the iterative process meanwhile benefiting from block sparsity and NC signal properties.

The notations used in this letter are described in Table I.

TABLE I: Notational Conventions

| | |
|--|---|
| $a, \mathbf{A}, \mathbf{a}, \mathbb{A}$ | Scalar, matrix, vector, and set |
| $\mathbf{A}^T, \mathbf{A}^*, \mathbf{A}^H, \mathbf{A}^{-1}$ | Transpose, conjugate, Hermitian-transpose and inversion of matrix \mathbf{A} |
| $\mathbf{A} = \text{diag}(a), \mathbf{A} = \text{blkdiag}(a)$ | Diagonal matrix and a block diagonal matrix with given elements |
| $[\mathbf{A}]_{i,:}, [\mathbf{A}]_{:,j}, [\mathbf{A}]_{i,j}$ | The elements of the i -th row, the elements of the j -th column, and the element in the i -th row and j -th column. |
| \mathbf{I}, \mathbf{O} | An identity matrix and a null matrix |
| $\text{Re}\{\mathbf{A}\}, \text{Im}\{\mathbf{A}\}$ | The real part and the imaginary part of the matrix |
| $ \mathbf{A} , \ \mathbf{a}\ _2, \ \mathbf{A}\ _F$ | The determinant of a matrix, the ℓ_2 -norm of a vector, and the Frobenius norm of a matrix |
| $\text{Tr}\{\mathbf{A}\}, \text{Toep}\{\cdot\}, \mathbb{E}\{\cdot\}$ | The trace of a matrix, a Toeplitz matrix with given elements and the mathematical expectation |
| $j = \sqrt{-1}, \mathcal{CN}(\cdot)$ | The imaginary unit and the complex Gaussian distribution |
| $\log(a), \Omega, \delta(a, b)$ | The natural logarithm with base e , the region of interest and the Kronecker delta function |

II. SIGNAL MODEL

A. NC signal model

Considering K far-field independent narrow-band signals impinging on a uniform linear array (ULA) with M sensors [19],

$$\mathbf{z}(t) = \mathbf{A}\mathbf{s}(t) + \mathbf{n}(t), t = 1, 2, \dots, L, \quad (1)$$

where $\mathbf{A} = [\mathbf{a}(\theta_1), \mathbf{a}(\theta_2), \dots, \mathbf{a}(\theta_K)] \in \mathbb{C}^{M \times K}$ with $\mathbf{a}(\theta_k) = [1, e^{-j\pi\sin\theta_k}, \dots, e^{-j(M-1)\pi\sin\theta_k}]^T$, $k = 1, 2, \dots, K$ and θ_k represents the DOA of the k -th source, L denotes the number of snapshots.

Collecting L snapshots, (1) can be written as

$$\mathbf{Z} = \mathbf{A}\mathbf{S} + \mathbf{N} \in \mathbb{C}^{M \times L}, \quad (2)$$

where $\mathbf{Z} = [\mathbf{z}(1), \dots, \mathbf{z}(L)]$, $\mathbf{S} = \Psi\mathbf{S}_R \in \mathbb{C}^{K \times L}$ is the strict NC signals [13], $\Psi = \text{diag}(e^{-j\phi_1}, \dots, e^{-j\phi_K}) \in \mathbb{C}^{K \times K}$ denotes the maximum noncircularity rate of signals and $\mathbf{S}_R = [\mathbf{s}_R(1), \dots, \mathbf{s}_R(L)]$ denotes the real part of signals.

The augmented received signal based on NC properties [13] is

$$\begin{aligned} \mathbf{Y} &= \begin{bmatrix} \mathbf{Z}^* \\ \mathbf{Z} \end{bmatrix} = \begin{bmatrix} \mathbf{A}^* & \mathbf{O} \\ \mathbf{O} & \mathbf{A} \end{bmatrix} \begin{bmatrix} \mathbf{S}^* \\ \mathbf{S} \end{bmatrix} + \begin{bmatrix} \mathbf{N}^* \\ \mathbf{N} \end{bmatrix} \\ &= \mathbf{B}\mathbf{S}_{\text{nc}} + \mathbf{W} \in \mathbb{C}^{2M \times L}, \end{aligned} \quad (3)$$

where $\mathbf{B} = \text{blkdiag}(\mathbf{A}^*, \mathbf{A}) \in \mathbb{C}^{2M \times 2K}$, $\mathbf{S}_{\text{nc}} = [\mathbf{S}^H, \mathbf{S}^T]^T$, $\mathbf{W} = [\mathbf{N}^H, \mathbf{N}^T]^T$.

B. On-grid sparse signal representation model

We only consider the SSR based model of NC signals under the on-grid condition. In this case for multiple sources, the region of interest (ROI) Ω is divided into a set of uniform discrete grid points (GPs) [9], denoted as $\mathcal{G} = \{\tilde{\theta}_n \mid n = 1, \dots, N\}$, where $N \gg K$. If all the source DOAs θ_k lie on the GPs, i.e., $\{\theta_k\}_{k=1}^K \subseteq \mathcal{G}$. \mathbf{Y} represents the received signal of $\bar{\mathbf{S}}$, and can be expressed as

$$\mathbf{Y} = \bar{\mathbf{B}}\bar{\mathbf{S}} + \mathbf{W}, \quad (4)$$

where $\bar{\mathbf{B}} = \text{blkdiag}(\bar{\mathbf{A}}^*, \bar{\mathbf{A}}) \in \mathbb{C}^{2M \times 2N}$, $\bar{\mathbf{A}} = [\mathbf{a}(\tilde{\theta}_1), \dots, \mathbf{a}(\tilde{\theta}_N)] \in \mathbb{C}^{M \times N}$. $\bar{\mathbf{S}} = [\tilde{\mathbf{S}}^H, \tilde{\mathbf{S}}^T]^T$, $\tilde{\mathbf{S}}$ is a row-sparse matrix, expressed as

$$[\tilde{\mathbf{S}}]_{n,\cdot} = \begin{cases} [\mathbf{S}]_{k,\cdot}, & \text{if } \tilde{\theta}_n = \theta_k, \\ \mathbf{0}, & \text{otherwise.} \end{cases} \quad (5)$$

III. PROPOSED ALGORITHM

A. Accurate block sparse signal model

The signal $\bar{\mathbf{S}}$, as shown in the left part of Fig. 1, does not yet possess block sparse characteristics but instead exhibits an element-wise sparsity pattern along its rows. Therefore, a permutation matrix \mathbf{J} is needed to reconstruct the manifold matrix, ensuring that the signal exhibits block-sparse characteristics.

Define $\mathbf{J} \in \mathbb{C}^{2N \times 2N}$ with its (i, j) -th entry expressed as

$$J_{i,j} = \delta(j, 2i - 1) \cdot \mathbf{1}_{i \leq N} + \delta(j, 2i - 2N) \cdot \mathbf{1}_{i > N}, \quad (6)$$

where $\mathbf{1}_{\text{condition}}$ denotes the indicator function, which equals 1 if the condition is true, and 0 otherwise.

By reconstructing the array manifold matrix, the NC signal is converted into a block-structured sparse signal, as shown in the right part of Fig. 1,

$$\mathbf{Y} = \bar{\mathbf{B}}\mathbf{J}\mathbf{X} + \mathbf{W} = \mathbf{V}\mathbf{X} + \mathbf{W}, \quad (7)$$

where $\mathbf{V} = \bar{\mathbf{B}}\mathbf{J}$, and the block sparse signal, denoted by \mathbf{X} , consists of N blocks $\mathbf{X}_i \in \mathbb{C}^{2 \times L}$, among which K blocks are non-zero. $\tilde{\theta}_i$ denotes the angle of the i -th block. That is

$$\mathbf{X}_i = \begin{cases} [e^{j\phi_k} \mathbf{S}_R^T, e^{-j\phi_k} \mathbf{S}_R^T]^T, & \text{if } \tilde{\theta}_i = \theta_k, \\ \mathbf{0}, & \text{otherwise.} \end{cases} \quad (8)$$

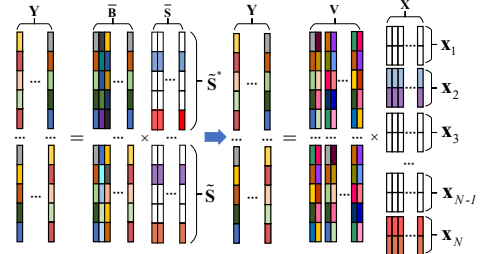


Fig. 1: Structure of block sparse signal model.

B. BSL framework for MMV model

The i -th block signal \mathbf{X}_i ($i = 1, 2, \dots, N$) can be modeled as [11]

$$p(\mathbf{X}_i; \{\gamma_i, \mathbf{G}_i\}) \sim \mathcal{CN}(\mathbf{X}_i; \mathbf{0}, \gamma_i \mathbf{G}_i), \quad (9)$$

where \mathbf{G}_i is a symmetric positive definite matrix that represents the correlation structure information within the signal block \mathbf{X}_i , γ_i is a hyperparameter that controls the sparsity of the block signal \mathbf{X}_i . Assuming the inter-blocks of sparsity signals are mutually independent, the signal can be written as [20]

$$p(\mathbf{X}; \boldsymbol{\Gamma}) = \prod_{i=1}^N p(\mathbf{X}_i; \{\gamma_i, \mathbf{G}_i\}) \sim \mathcal{CN}(\mathbf{X}; \mathbf{0}, \boldsymbol{\Gamma}), \quad (10)$$

where $\boldsymbol{\Gamma} = \text{diag}(\gamma_1 \mathbf{G}_1, \dots, \gamma_N \mathbf{G}_N) \in \mathbb{C}^{2N \times 2N}$, and the weight vector $\boldsymbol{\gamma} = [\gamma_1, \gamma_2, \dots, \gamma_N]^T$.

\mathbf{W} is an additive Gaussian white noise matrix, following a Gaussian distribution with a zero mean and variance β^{-1} [9],

$$p(\mathbf{W}) \sim \mathcal{CN}(\mathbf{0}, \beta^{-1} \mathbf{I}). \quad (11)$$

Therefore, the observation matrix \mathbf{Y} follows a Gaussian distribution with a mean of $\mathbf{V}\mathbf{X}$ and variance $\beta^{-1}\mathbf{I}$ [10],

$$\begin{aligned} p(\mathbf{Y}|\mathbf{X}; \beta) &\sim \mathcal{CN}(\mathbf{Y}; \mathbf{V}\mathbf{X}, \beta^{-1}\mathbf{I}) \\ &= (\pi\beta^{-1})^{-NL} \exp\{-\beta\|\mathbf{Y} - \mathbf{V}\mathbf{X}\|_F^2\}. \end{aligned} \quad (12)$$

According to the law of total probability, the likelihood function can be derived as follows

$$p(\mathbf{Y}; \boldsymbol{\Gamma}) = \int_{\mathbf{X}} p(\mathbf{Y}|\mathbf{X})p(\mathbf{X}; \boldsymbol{\Gamma})d\mathbf{X}. \quad (13)$$

The integral in (13) can be interpreted as the convolution of two Gaussian functions, and the result still follows a Gaussian distribution [20]

$$p(\mathbf{Y}|\boldsymbol{\Gamma}, \beta) \sim \mathcal{CN}(\mathbf{Y}; \mathbf{0}, \mathbf{C}), \quad (14)$$

where $\mathbf{C} = \mathbb{E}\{\mathbf{Y}\mathbf{Y}^H\} = \beta^{-1}\mathbf{I} + \mathbf{V}\mathbf{V}^H$.

According to the Bayes rule, the posterior $p(\mathbf{X}|\mathbf{Y}; \Gamma, \beta)$ can be expressed as [20]

$$p(\mathbf{X}|\mathbf{Y}; \Gamma, \beta) \propto p(\mathbf{Y}|\mathbf{X}; \beta)p(\mathbf{X}; \Gamma) \\ \propto \frac{\exp\{-\text{Tr}[(\mathbf{X} - \boldsymbol{\mu})^H \boldsymbol{\Sigma}^{-1}(\mathbf{X} - \boldsymbol{\mu})]\}}{(\pi^N |\boldsymbol{\Sigma}|)^L} \sim \mathcal{CN}(\boldsymbol{\mu}, \boldsymbol{\Sigma}), \quad (15)$$

where

$$\boldsymbol{\mu} = \beta \boldsymbol{\Sigma} \mathbf{V}^H \mathbf{Y} \in \mathbb{C}^{2N \times L}, \quad (16)$$

$$\boldsymbol{\Sigma} = (\Gamma^{-1} + \beta \mathbf{V}^H \mathbf{V})^{-1} \in \mathbb{C}^{2N \times 2N}. \quad (17)$$

To estimate the parameters $\{\gamma_i, \mathbf{G}_i\}$ and β , a Type-II maximum likelihood method can be used to obtain the cost function $\mathcal{L}(\Theta)$ [11],

$$\mathcal{L}(\Theta) = -2\log p(\mathbf{Y}|\Gamma, \beta) \propto L \log |\mathbf{C}| + \text{Tr}(\mathbf{Y}^H \mathbf{C}^{-1} \mathbf{Y}). \quad (18)$$

where $\Theta \triangleq \{\beta, \{\gamma_i, \mathbf{G}_i\}_{i=1}^N\}$ denotes a set of estimated parameters.

C. Fast Marginal Likelihood Maximization

In BSBL methods, parameter updates involve iterative algorithms with matrix inversion (17), yielding $\mathcal{O}(8N^3)$ complexity. Using the Woodbury identity reduces it to $\mathcal{O}(8M^3)$, however, the computational cost is forbidden. To address this issue, the FMLM concept is introduced [10], where basis functions are iteratively added and removed until all non-zero weights are included.

\mathbf{C} in (14) can be rewritten as [10]

$$\mathbf{C} = \beta^{-1} \mathbf{I} + \sum_{n \neq i} \mathbf{V}_n \mathbf{L}_n \mathbf{V}_n^H + \mathbf{V}_i \mathbf{L}_i \mathbf{V}_i^H \\ = \mathbf{C}_{-i} + \mathbf{V}_i \mathbf{L}_i \mathbf{V}_i^H, \quad i = 1, 2, \dots, N, \quad (19)$$

where $\mathbf{L}_i \triangleq \gamma_i \mathbf{G}_i \in \mathbb{C}^{2 \times 2}$ [21], $\mathbf{C}_{-i} \triangleq \beta^{-1} \mathbf{I} + \sum_{n \neq i} \mathbf{V}_n \mathbf{L}_n \mathbf{V}_n^H$ is obtained by removing the i -th basic function from \mathbf{C} . $\mathbf{V}_i \in \mathbb{C}^{2M \times 2}$ denotes basis functions corresponding to the i -th signal block.

Substituting the decomposition (19) into the cost function (18), resulting in

$$\mathcal{L}(\Theta) = L \log |\mathbf{C}_{-i}| + \text{Tr}[\mathbf{Y}^H \mathbf{C}_{-i}^{-1} \mathbf{Y}] + L \log |\mathbf{I} + \mathbf{L}_i \mathbf{V}_i^H \mathbf{C}_{-i}^{-1} \mathbf{V}_i| \\ - \text{Tr}\{\mathbf{Y}^H \mathbf{C}_{-i}^{-1} \mathbf{V}_i (\mathbf{L}_i^{-1} + \mathbf{V}_i^H \mathbf{C}_{-i}^{-1} \mathbf{V}_i)^{-1} \mathbf{V}_i^H \mathbf{C}_{-i}^{-1} \mathbf{Y}\}. \quad (20)$$

Let $\mathbf{U}_i \triangleq \mathbf{V}_i^H \mathbf{C}_{-i}^{-1} \mathbf{V}_i$, $\mathbf{Q}_i \triangleq \mathbf{V}_i^H \mathbf{C}_{-i}^{-1} \mathbf{Y}$, (20) can be further simplified as

$$\mathcal{L}(\Theta) = L \log |\mathbf{C}_{-i}| + \text{Tr}[\mathbf{Y}^H \mathbf{C}_{-i}^{-1} \mathbf{Y}] \\ + L \log |\mathbf{I} + \mathbf{L}_i \mathbf{U}_i| - \text{Tr}\{\mathbf{Q}_i^H (\mathbf{L}_i^{-1} + \mathbf{U}_i)^{-1} \mathbf{Q}_i\} \\ = \mathcal{L}(-i) + \mathcal{L}(i), \quad (21)$$

where $\mathcal{L}(i) \triangleq L \log |\mathbf{I} + \mathbf{L}_i \mathbf{U}_i| - \text{Tr}\{\mathbf{Q}_i^H (\mathbf{L}_i^{-1} + \mathbf{U}_i)^{-1} \mathbf{Q}_i\}$.

The update of \mathbf{L}_i only depends on $\mathcal{L}(i)$. To optimize $\mathcal{L}(\Theta)$, we set $\frac{\partial \mathcal{L}(i)}{\partial \mathbf{L}_i} = \mathbf{O}$. The update rule of \mathbf{L}_i is formulated as

$$\mathbf{L}_i = \mathbf{U}_i^{-1} \left(\frac{\mathbf{Q}_i \mathbf{Q}_i^H}{L} - \mathbf{U}_i \right) \mathbf{U}_i^{-1}. \quad (22)$$

Thus, the intra-block correlation γ_i is given by [21]

$$\gamma_i = \frac{1}{2} \text{Tr}(\mathbf{L}_i). \quad (23)$$

Update the correlation structure matrix $\mathbf{G}_i = \mathbf{L}_i / \gamma_i$.

The convergence condition of the algorithm is satisfied when the normalized change rate $\epsilon = \frac{\|\boldsymbol{\gamma}^{\text{new}} - \boldsymbol{\gamma}^{\text{old}}\|_2}{\|\boldsymbol{\gamma}^{\text{old}}\|_2}$ falls below the predefined threshold ϵ_{\min} , or when the maximum number of iterations is reached.

D. Block structure factors and noise value estimation.

For block-sparse models of NC signals, further constraints on \mathbf{G}_i can enhance algorithm performance due to the fixed block size [19]. A first-order autoregressive (AR) model is used in \mathbf{G}_i to efficiently capture intra-block correlations along the main and sub-diagonals while reducing computation [11],

$$\mathbf{G}_i = \text{Toeplitz}([1, r]), \quad (24)$$

the AR factor r is defined as $r \triangleq \frac{m_1}{m_0}$, where m_1 and m_0 represents the mean value of the elements on the main diagonal and the sub-diagonal of \mathbf{G}_i respectively.

The noise parameter β^{-1} can be estimated using the following formula

$$\beta = \frac{M}{\text{Tr}[\boldsymbol{\Sigma} \mathbf{V}^H \mathbf{V}] + \|\mathbf{Y} - \mathbf{V}\mathbf{X}\|_F^2}. \quad (25)$$

However, in practical applications, updating β can lead to instability in signal reconstruction performance [21]. Therefore, β is considered a constant set manually as $\beta^{-1} = 0.01 \|\mathbf{Y}\|_F^2$.

E. DOA and NC phases estimation

The hyperparameter $\boldsymbol{\gamma}$ from (23) determines the sparse signal's power distribution, enabling the reconstruction of $\hat{\mathbf{X}}$, where $\hat{\mathbf{X}}_i \in \mathbb{C}^{2 \times L}$ represents the n -th block. The spectral function is then given as

$$\mathbf{P}(\tilde{\theta}_n) = \frac{1}{L} \left(\sum_{l=1}^L |\hat{\mathbf{X}}_{i,1,l}| + \sum_{l=1}^L |\hat{\mathbf{X}}_{i,2,l}| \right), \quad (26)$$

where $\hat{\mathbf{X}}_{i,1,l}$ and $\hat{\mathbf{X}}_{i,2,l}$ represent the l -th sample data in the first and second rows of the n -th block, respectively. The K largest spectral peaks, identified via a spectral peak search, correspond to the desired DOA values.

The proposed algorithm estimates the DOA and recovers the k -th NC phase from the reconstructed signal $\hat{\mathbf{X}}$, with the estimation formula given by

$$\hat{\phi}_k = \frac{\sum_{l=1}^L \arctan(\text{Im}(\hat{\mathbf{X}}_{k,1,l}) / \text{Re}(\hat{\mathbf{X}}_{k,1,l}))}{L}, \quad (27)$$

where $\hat{\mathbf{X}}_k$ represents the block signal corresponding to the k -th spectral peak. The algorithm flow is presented in Algorithm 1.

IV. NUMERICAL SIMULATION

This section compares the proposed algorithm with NC-PM [14], NC-ESPRIT [15], SBL [20], and its variant adapted for NC signals (NC-SBL), which assumes known NC phase information incorporated into the overcomplete dictionary \mathcal{G} .

The experimental setup includes $M = 12$ array elements, $L = 20$ snapshots, an overcomplete dictionary $\mathcal{G} = [-40 : 10 : 90]$

Algorithm 1 NC-BSBL

```

1: Input:  $\mathbf{Y}$ ,  $\bar{\mathbf{B}}$ ,  $\mathbf{J}$ , obtain  $\mathbf{V}$  from (7).
2: Initialization: Initialize  $\mathbf{G}_i = \mathbf{I}$ ,  $\mathbf{L}_i = \mathbf{O}$ ,  $\mathbf{U}_i = \beta \mathbf{V}^H \mathbf{V}$ ,  $\mathbf{Q}_i = \beta \mathbf{V}^H \mathbf{Y}$ , set
parameters Maxiter = 500 and  $\epsilon_{\min} = 10^{-4}$ .
3: while  $\epsilon > \epsilon_{\min}$  and iter < Maxiter do
4:   Update  $\mathbf{L}_i$ ,  $\gamma_i$ ,  $\mathbf{G}_i$  (22), (23), (24).
5:   Compute  $\Delta \mathcal{L}(i) = \mathbf{L}(\gamma_i \mathbf{G}_i) - \mathcal{L}(\mathbf{L}_i)$  for all blocks and select  $\hat{i}$ -th block
suck that  $\Delta \mathcal{L}(\hat{i}) = \min\{\mathcal{L}(i)\}$ .
6:   Update  $\boldsymbol{\mu}$ ,  $\boldsymbol{\Sigma}$  based on (16), (17).
7:   iter = iter + 1.
8: end while
9: Compute spectral peak  $\mathbf{P}(\tilde{\theta}_n)$  (26) and NC phases (27).
10: Output: DOA parameters  $\hat{\theta}$  and NC phases  $\hat{\phi}$ .

```

$0.1 : 40]^\circ$ with $N = 801$ grid points, $\epsilon_{\min} = 10^{-4}$, and a maximum of 500 iterations. NC-SBL requires identical NC phases $\Psi_1 = [\pi/12, \pi/12]$, while NC-BSBL adapts for arbitrary NC phases $\Psi_2 = [\pi/12, \pi/4]$. $\theta = [10^\circ, 30^\circ]$.

We employ the root mean square error (RMSE) as a metric to evaluate the accuracy of DOA and NC phases estimation, which is defined as [13]

$$\text{RMSE} = \sqrt{\frac{1}{K} \frac{1}{T} \sum_{k=1}^K \sum_{t=1}^T (\hat{\xi}_{t,k} - \xi_k)^2}. \quad (28)$$

where $\hat{\xi}_{t,k}$ denotes the estimated DOA (NC phases) parameter for the k -th source in the t -th trial, while ξ_k represents its true value of the k -th source. The number of trials for the Monte Carlo simulation is set to $T = 500$. The Cramér-Rao Bound (CRB) [22] is utilized to assess the algorithm's performance.

Table II presents the average CPU time required for 500 runs of the algorithm under SNR = 10dB. It can be observed that the NC-BSBL algorithm significantly reduces the computation time due to the incorporation of the FMLM method.

TABLE II: Average CPU time for 500 runs of algorithms.

| Algorithm | Average CPU Time (Seconds) |
|------------------|----------------------------|
| NC-BSBL (FMLM) | 0.1165 |
| SBL (No FMLM) | 2.1516 |
| NC-SBL (No FMLM) | 2.3236 |

Fig. 2 presents the spectral peaks of NC-BSBL, NC-SBL, and SBL. It can be observed that NC-BSBL produces fewer spurious peaks, with sharper peaks at the correct DOAs, indicating that the proposed algorithm achieves more accurate estimates compared to the others.

Fig. 3 illustrates the estimation error of various algorithms across SNRs from -5dB to 20dB. While noncircularity increases signal dimensionality and amplifies noise, impacting FMLM's basis selection and performance [10], NC-BSBL shows higher errors at low SNRs. However, at high SNRs (e.g., above 15dB), it surpasses SBL and NC-SBL by leveraging NC properties and intra-block correlations for enhanced accuracy.

Fig. 4 illustrates the RMSE of NC-BSBL for NC phases recovery under single-source ($\theta = 10^\circ$, $\phi = \pi/4$) and two-source ($\theta = [10^\circ, 30^\circ]$, $\Psi = [\pi/12, \pi/4]$) scenarios. As SNR increases, improved source reconstruction enhances NC phase recovery, validating the algorithm's effectiveness in estimating unknown and distinct NC phases.

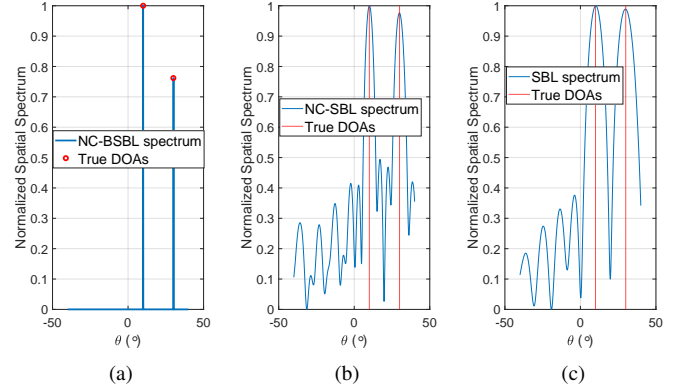


Fig. 2: Spectral peaks for two NC signals, $\theta = [10^\circ, 30^\circ]$, $\Psi_1 = [\pi/12, \pi/12]$ (known for NC-SBL), $\Psi_2 = [\pi/12, \pi/4]$ (unknown for NC-BSBL), $M = 12$, SNR = 10 dB, $L = 20$. (a) NC-BSBL. (b) NC-SBL. (c) SBL.

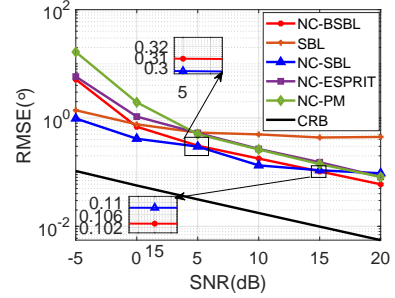


Fig. 3: The RMSE curves as a function of SNR with $M = 12$, $L = 20$, $\theta = [10^\circ, 30^\circ]$, and $\Psi_1 = [\pi/12, \pi/12]$ (known for NC-SBL), $\Psi_2 = [\pi/12, \pi/4]$ (unknown for NC-BSBL), $T = 500$.

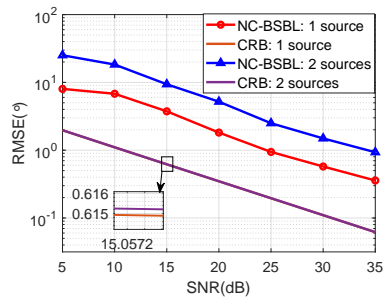


Fig. 4: The curve of RMSE versus SNR for NC phases, with $M = 12$, $L = 20$, $T = 500$.

V. CONCLUSION

This letter has proposed a DOA estimation algorithm for NC signals in the BSBL framework, leveraging noncircularity and block sparsity without prior NC phase. The permutation matrix reorganizes signal components to capture intra-block information, improving recovery. Future work will refine block constraints via NC conjugate symmetry and integrate off-grid techniques for greater precision.

REFERENCES

- [1] R. Schmidt, "Multiple emitter location and signal parameter estimation," *IEEE Transactions on Antennas and Propagation*, vol. 34, no. 3, pp. 276–280, 1986.
- [2] R. Roy, A. Paulraj, and T. Kailath, "ESPRIT—A subspace rotation approach to estimation of parameters of cisoids in noise," *IEEE Transactions on Acoustics, Speech, and Signal Processing*, vol. 34, no. 5, pp. 1340–1342, 1986.
- [3] D. Veerendra, K. R. Niranjan, I. Malik, A. Khandare, M. Patil, T. S. Kishore, K. S. Balamurugan, K. R. Pedada, and A. Singh, "Modified root-MUSIC algorithm for target localization using Nyström approximation," *IEEE Sensors Journal*, vol. 24, no. 8, pp. 13209–13216, 2024.
- [4] Z. Tang, K. Zhou, Y. Xu, P. Meng, and H. Zhang, "An estimation method for soft fault reflection coefficient of power cable based on sliding-window TLS-ESPRIT," *IEEE Transactions on Power Delivery*, vol. 39, no. 6, pp. 3092–3100, 2024.
- [5] Q. Shen, W. Liu, W. Cui, and S. Wu, "Underdetermined DOA estimation under the compressive sensing framework: A Review," *IEEE Access*, vol. 4, pp. 8865–8878, 2016.
- [6] C. Niu, T. Lv, Y. Liu, X. Wang, and J. Jin, "A DOA estimation method for coherent signals based on weighted l_1 -SVD," in *2023 IEEE 6th International Conference on Electronic Information and Communication Technology (ICEICT)*, 2023, pp. 694–699.
- [7] Y. Song, F. Wu, Y. Ni, and K. Yang, "A fast threshold OMP based on self-learning dictionary for propeller signal reconstruction," *Ocean Engineering*, vol. 287, p. 115792, 2023.
- [8] R. R. Pote and B. D. Rao, "Maximum likelihood-based gridless DOA estimation using structured covariance matrix recovery and SBL with grid refinement," *IEEE Transactions on Signal Processing*, vol. 71, pp. 802–815, 2023.
- [9] J. Li, X. Dong, X. Shi, and X. Zhang, "An enhanced direct position determination of non-circular sources via sparse Bayesian inference and grid refinement strategy," *Digital Signal Processing*, vol. 151, p. 104564, 2024.
- [10] Y. Mao, Q. Guo, J. Ding, F. Liu, and Y. Yu, "Marginal likelihood maximization based fast array manifold matrix learning for direction of arrival estimation," *IEEE Transactions on Signal Processing*, vol. 69, pp. 5512–5522, 2021.
- [11] Z. Zhang and B. D. Rao, "Extension of SBL algorithms for the recovery of block sparse signals with intra-block correlation," *IEEE Transactions on Signal Processing*, vol. 61, no. 8, pp. 2009–2015, 2013.
- [12] Z. Zhang and B. D. Rao, "Sparse signal recovery with temporally correlated source vectors using sparse Bayesian learning," *IEEE Journal of Selected Topics in Signal Processing*, vol. 5, no. 5, pp. 912–926, 2011.
- [13] X. Dong, M. Sun, J. Zhao, X. Zhang, and Y. Wang, "Enhanced BNC approach for noncircular signals direction finding with sparse array in the scenario of impulsive noise," *IEEE Transactions on Aerospace and Electronic Systems*, vol. 59, no. 5, pp. 6265–6277, 2023.
- [14] X. Chen, C. Wang, and X. Zhang, "DOA and noncircular phase estimation of noncircular signal via an improved noncircular rotational invariance propagator method," *Mathematical Problems in Engineering*, vol. 2015, no. 1, p. 235173, 2015.
- [15] W. Zheng, X. Zhang, H. Sun, and R. Cao, "Non-circular generalised-ESPRIT algorithm for direction of arrival estimation," *IET Radar, Sonar & Navigation*, vol. 11, no. 5, pp. 736–744, 2017.
- [16] J. Zhang, T. Qiu, and S. Luan, "An efficient real-valued sparse Bayesian learning for non-circular signal's DOA estimation in the presence of impulsive noise," *Digital Signal Processing*, vol. 106, p. 102838, 2020.
- [17] J. Pan, H. Pan, M. Sun, Y. Wang, V. Baltazart, X. Dong, J. Zhao, X. Zhang, and H. C. So, "Co-prime sampling-based time-delay estimation for roadway survey by ground penetrating radar via off-grid sparse Bayesian learning," *IEEE Transactions on Radar Systems*, vol. 2, pp. 966–978, 2024.
- [18] J. Yuan, G. Zhang, H. Leung, and S. Ma, "Off-grid DOA estimation for noncircular signals via block sparse representation using extended transformed nested array," *IEEE Signal Processing Letters*, vol. 30, pp. 130–134, 2023.
- [19] Y. Jin, D. He, S. Wei, and W. Yu, "Off-grid DOA estimation method based on sparse Bayesian learning with clustered structural-aware prior information," *IEEE Transactions on Vehicular Technology*, vol. 73, no. 4, pp. 5469–5483, 2024.
- [20] P. Gerstoft, C. F. Mecklenbräuker, A. Xenaki, and S. Nannuru, "Multi-snapshot sparse Bayesian learning for DOA," *IEEE Signal Processing Letters*, vol. 23, no. 10, pp. 1469–1473, 2016.
- [21] B. Liu, Z. Zhang, G. Xu, H. Fan, and Q. Fu, "Energy efficient telemonitoring of physiological signals via compressed sensing: A fast algorithm and power consumption evaluation," *Biomedical Signal Processing and Control*, vol. 11, pp. 80–88, 2014.
- [22] J. Steinwandt, F. Roemer, M. Haardt, and G. Del Galdo, "Deterministic Cramér-rao Bound for strictly non-circular sources and analytical analysis of the achievable gains," *IEEE Transactions on Signal Processing*, vol. 64, no. 17, pp. 4417–4431, 2016.